In chronic pancreatitis CD25+/Foxp3+ regulatory T-cells control pancreatic fibrosis by suppression of the type 2 immune response

Juliane Glaubitz
University Medicine Greifswald
Anika Wilden
University Medicine Greifswald
Janine Golchert
University Medicine Greifswald
Georg Homuth
University Medicine Greifswald
Uwe Voelker
University Medicine Greifswald https://orcid.org/0000-0002-5689-3448
Barbara Bröker
University Medicine Greifswald
Markus Lerch
University Medicine
Julia Mayerle
Ernst-Moritz-Arndt-University Greifswald
Ali Aghdassi
University Medicine
Frank Weiss
University Medicine Greifswald
Matthias Sendler (matthias.sendler@uni-greifswald.de)
University Medicine Greifswald

Article

Keywords: Chronic pancreatitis (CP), T-cells, chronic pancreatitis, immune response

Posted Date: July 13th, 2021

DOI: https://doi.org/10.21203/rs.3.rs-666070/v1

Version of Record: A version of this preprint was published at Nature Communications on August 3rd, 2022. See the published version at https://doi.org/10.1038/s41467-022-32195-2.

Abstract

Chronic pancreatitis (CP) is characterized by chronic inflammation and the progressive fibrotic replacement of exocrine and endocrine pancreatic tissue. We identified Tregs as central regulators of the fibroinflammatory reaction by a selective depletion of Foxp3-positive cells in a transgenic mouse model (DEREG-mice) of experimental CP. In Treg-depleted DEREG-mice, the induction of CP resulted in a significantly increased stroma deposition, the development of exocrine insufficiency and significant weight loss starting from day 14 after disease onset. In CP, Foxp3+/CD25+ Tregs suppress the type-2 immune response by a repression of Gata3+ T-helper cells (Th2), Gata3+ innate lymphoid cells type 2 (ILC2) and CD206+ M2-macrophages. A suspected pathomechanism behind the fibrotic tissue replacement may involve an observed dysbalance of Activin A expression in macrophages and of its counter regulator Follistatin. Our study identified Tregs as key regulators of the type-2 immune response and of organ remodeling during CP. The Treg-triggered immune response could be a therapeutic target to prevent fibrosis and preserve functional pancreatic tissue.

Introduction

Chronic pancreatitis (CP) is a common gastrointestinal disease, characterized by a progressive inflammatory process of the pancreas which leads to irreversible fibrotic replacement of exocrine and endocrine tissue. These morphologic alterations which finally cause pancreatic insufficiency[1] and diabetes mellitus are often accompanied by chronic pain[2] and significantly affect the quality of life of patients[3]. As chronic pancreatitis cannot be cured, symptomatic treatment is directed toward relieving pain, improving malabsorption, and treatment of diabetes mellitus[4].

Intrapancreatic activation of digestive enzymes is associated with acinar cell death and represents an initial triggering event in the onset and progression of CP[5–7]. The activation of a pro-inflammatory immune reaction contributes to pancreatic damage[8–10], and cells of the innate immune system, like monocytes/macrophages and neutrophils, infiltrate the damaged pancreas[9–11]. Especially macrophages represent a cell population of the innate immune system with vast plasticity executing different tasks, and therefore play a crucial role in acute[9,10] as well as chronic forms [12,13] of pancreatitis. Recent data illustrate how the disease progresses from pro-inflammation in the acute phase to tissue repair and fibrosis[14,15] in the regeneration phase. Alternatively activated macrophages are suggested to be the key mediators of fibrogenesis and tissue regeneration[13]. They are characterized by the release of transforming growth factors TGF-β, TGF-α, platelet derived growth factor PDGF[16] or the anti-inflammatory cytokine IL-10[17] and promote wound healing and fibrogenesis[18]. Quiescent pancreatic stellate cells (PSC) are activated by TGF-β[19] and produce extracellular matrix proteins like type I and type III collagens[20]. Excessive activation of PSC may favor tissue fibrosis over tissue repair and can result in the loss of exocrine and endocrine tissue. In pancreatitis, fibrotic tissue replacement is associated with a type 2immune response[21,22]. Simultaneously with the pro-inflammatory local response within the damaged pancreas, a systemic counter regulation that prevents hyperinflammation is activated[22].

Foxp3+/CD25+ regulatory T-cells (Tregs) are known cellular players balancing the immune response and preventing excessive inflammatory reactions[23] which act on cells of the innate as well as the adaptive immune system[24] and represent regulators of tissue repair processes[25]. CP is characterized by a prominent type 2 immune response[26] involving Th2 cells and alternatively activated macrophages *via* the IL-4/IL-13 axis[22]. Here, we investigated the role of Foxp3+/CD25+ Tregs in a mouse model of chronic pancreatitis using DEREG mice which were depleted of regulatory T-cells[27]. In the present study we demonstrate that suppression of the type 2 immune response actioned by Tregs is indispensable to prevent tissue destruction and pancreatic fibrogenesis.

Results

CP is associated with an activation of Tregs and a type 2 immune response

CP was induced by repetitive caerulein injections over four weeks in C57Bl/6 mice. Animals were sacrificed 3d after the last caerulein treatment. Tissue sections of CP mice showed increased numbers of alternatively activated CD206+ macrophages accompanied by prominent collagen 1 staining, indicating fibrotic scarring (**Fig. 1a**). We also analyzed splenic lymphocytes of the mice by flow cytometry but observed only a slight non-significant increase in CD206+/CD11b+/Ly6G- macrophages (**Fig. 1b**). In line CD163+, a second marker of alternatively activated macrophages, remain stable in CP mice and untreated controls (con) (**Fig. 1c**). With regard to the adaptive immune system we observed a significant increase of Foxp3+/CD25+ regulatory T-cells (**Fig. 1d**) and Gata3+ Th2 cells (**Fig. 1e**), whereas Tbet+ Th1 cell numbers were not elevated in the spleen (**Fig. 1f**). CP was also induced in DEpletion of REGulatory T cell (DEREG) mice that express a diphtheria toxin receptor (DTR)-eGFP fusion transgene under the control of the Foxp3 promoter[27]. This allows to detect Tregs by anti-GFP immunofluorescent labeling. Of note, we were able to detect sporadic CD3+/GFP positive Tregs in the pancreas of DEREG mice after induction of chronic pancreatitis (**Fig. 1g**). Under these conditions, macrophages enter the damaged organ or are activated therein, whereas the activation of T-cells occurs within the lymphatic system, only occasional T-cells could be detected in the damaged pancreas.

Tregs suppress the splenic type 2 immune response during CP

We next investigated the role of regulatory T-cells during CP. In DEREG mice, Tregs are selectively depleted by diphtheria toxin (DT) administration because these mice express the gene encoding a diphtheria toxin receptor DTR-eGFP under the *Foxp3* promoter[27]. A DEREG control group received phosphate buffered saline (PBS) instead of DT. The success of Treg depletion was analyzed in lymph node sections by labeling the GFP+ Tregs with an anti-GFP antibody and in spleen cell suspensions by flow cytometric analysis of GFP+/CD4+ cells **(Fig. 2a and 2b)**. In both organs Tregs were strongly reduced after DT injection. Increased levels of CD69, a general activation marker of CD4+ T-cells, indicated significant T-effector cell activation in DT-treated mice (**Fig. 2c**). The polarity of the T-effector cell response (Th1/Th2 balance) was studied by flow cytometric analysis of the expression of the transcription factors Tbet and Gata3. Treg depletion during CP induction did not change the Th1 response (**Fig. 2d**), but it almost tripled

the percentage of Gata3+ Th2 cells in the spleen (**Fig. 2e**). Corroborating this finding, IL-4 and IL-10, cytokines which accompany a Th2/type 2 immune response, were significantly elevated in the serum of DT-treated mice. On the other hand, pro-inflammatory cytokines like IL6 were not significantly affected by the depletion of Foxp3+ Tregs (**Fig. 2f**). In line with the elevated Th2 response we observed an increased number of CD11b+/CD206+ macrophages in the spleen of DT-treated DEREG mice (**Fig. 2g**).

Tregs suppress the response of fibrogenic pancreatic CD206+ macrophages in CP

The systemic type 2 immune response is suppressed by Foxp3+/CD25+ Tregs and therefore significantly increased in their absence. Labeling of CD206+ macrophages in pancreatic tissue sections demonstrated that this also affects the pancreas (**Fig. 3a**), where significantly increased numbers of CD206+ macrophages could be detected in DT-treated animals with CP (**Fig. 3b**). Gene expression analysis of the alternative activated macrophage markers MRC-1 and YM1 in pancreatic tissue **(Fig. 3c)** and flow cytometry of isolated pancreatic leukocytes (**Fig. 3d**) confirmed the increase of CD206+ macrophages in DT-treated mice. Expression of *Il10* encoding cytokine IL-10 that is mainly released by CD206+ macrophages was increased in pancreatic tissue of DT-treated mice with CP. In contrast, the gene expression of the M1 macrophage-related cytokine IL-1β was not affected by the depletion (**Fig. 3e**). Macrophage differentiation towards alternatively activated anti-inflammatory M2-like phenotype correlates with an increased number as well as activation of pancreatic stellate cells. Labeling of α smooth muscle actin (αSMA) demonstrated increased numbers of activated stellate cells in the pancreas of Treg-depleted animals accompanied by increased expression of *Col1a1* encoding the extracellular matrix protein collagen 1 **(Fig. 3f)**. Flow cytometric analysis of cells isolated from CP tissue of DEREG mice demonstrated that systemic depletion of Tregs during CP resulted in a significant increase of cells positive for the stellate cell markers CD271 and GFAP **(Fig. 3g and 3h)**. Additional gene expression analysis of αSMA confirmed this finding **(Fig. 3i)**. Treg depletion enhanced pancreatic fibrosis which is visible in histological staining with Masson Goldner or Azan blue (**Fig. 3j**). The fibrotic cell area in relation to the total tissue area is significantly enlarged in Treg-depleted mice (**Fig. 3k and 3l**). A significant reduction of exocrine tissue area (surrounded in red) was detected in pancreatic sections from DT-treated animals (**supplement fig. 1a**). Immunofluorescent labeling with anti-cytokeratin 19 antibody revealed increased numbers of ductal structures, suggesting an increased acinar to ductal metaplasia in the DT-treated mice. (**supplement fig. 1b**).

Tregs regulate organ remodeling during CP

Aside from fibrotic tissue replacement, acinar cell regeneration plays a decisive role in organ remodeling in the course of CP. As macrophages are known to influence organ regeneration[15], we investigated the release of growth factors and growth factor related proteins from them in an *in vitro* co-culture model of bone marrow derived macrophages (BMDM) and CCK stimulated acini, as previously described[10]. After 6h of co-culture, the BMDMs were carefully washed, total RNA was prepared and subsequently used for transcriptome analyses using Affymetrix arrays. We observed increased mRNA levels of genes encoding

various growth factors like nerval growth factor (NGF), inhibin βa (INHBA), fibroblast growth factor 1 (FGF1), Amphiregulin (AREG) but also of counter regulators like follistatin (FST) (**Fig. 4a**).

Next, we studied organ regeneration by analyzing the gene expression of these growth factors and their inhibitors by RT-qPCR using RNA prepared from the pancreas of DEREG mice with CP.

In the pancreas of DT-treated Treg depleted mice there was elevated expression of the INHBA encoding the inhibin encoding subunit β_A subunit of the growth factor activin. The transcription of INHA that encoding the inhibin α subunit was not affected (**Fig. 4b**). Activin is a homodimer of the inhibin β_A subunit, whereas its inhibitory counterpart inhibin represents a heterodimer of inhibin α and inhibin β_A. Our results suggest an increased formation of homo-dimeric activin at the expense of the heterodimeric inhibin. Concomitantly the activin counter regulator follistatin was downregulated in the pancreas of DT-treated mice (**Fig. 4b**). These results are in line with the results of our *in vitro* co-culture experiments (**Fig. 4a**). Immunofluorescent labeling of CD206+ macrophages and of the inhibin βA subunits demonstrated co-localization of both markers in fibrotic areas of the pancreas with increased fluorescence signals in the absence of Tregs (**Fig. 4c**). The expression of FGF1 and TGFβ were also elevated in the pancreas of these mice (**Fig. 4d**). Both are known to activate pancreatic stellate cells[19], and to stimulate the production of extracellular matrix proteins like collagens. Collagen 1 which was also significantly elevated both at the mRNA (**Fig. 4d**) and protein levels (**Fig. 4c**). The immune labeling analysis of fibroblast growth factor receptor revealed co-localization with αSMA expressing PSCs (**Fig. 4e**). Our results show that in CP regulatory T-cells suppress the excessive release of growth factors by pancreatic macrophages, thereby limiting the fibrotic replacement of exocrine pancreatic tissue.

Tregs suppress innate lymphoid cells type 2

Besides Th2-cells and alternatively activated macrophages innate lymphoid cells type 2 (ILC2) are involved in the type 2 immune response. We therefore reasoned that ILC2s might also be regulated by Tregs during CP. First we investigated ILC2s in the spleen of DEREG mice with CP. Innate lymphoid cells are characterized by the absence of specific linage markers (lin-) but presence of CD45, CD127 and CD90 (**supplement. fig. 1**). The absence of Tregs did not result in an increase of total ILCs in the spleen (**Fig. 5a**). When we discriminated ILCs *via* the expression of the transcription factors Tbet and Gata3 into ILC subpopulations of type 1 and type 2 (**Fig. 5b**), comparable to the differentiation of T-cells, we observed a shift towards ILC2 differentiation, similar to the increased Th2 differentiation. Whereas the numbers of Tbet+ ILC1s did not change after DT treatment, those of Gata3+ ILC2s increased significantly (**Fig. 5c and 5d**). ILC2s are known to play a crucial role in tissue fibrosis[28,29]. Therefore, we next asked whether ILCs were present locally in pancreatic tissue during CP and whether these were also regulated by Tregs. We were able to detect lin- CD45+/CD127+/CD90+ cells by flow cytometry analysis of isolated pancreatic leukocytes (**Fig. 5e**). Animals suffering from CP showed an increase of ILCs in the pancreas that was significantly enhanced in DT-treated mice. The ILCs that are significantly increased in the absence of Tregs strongly express Gata3, which identifies them as ILC2s. **(Fig. 5f)**. ILC2 are characterized by the expression of amphiregulin (AREG), a transmembrane glycoprotein which belongs to the epidermal

growth factor family. Expression analysis of the encoding AREG gene in pancreas tissue by quantitative RT-qPCR revealed a significant increase in DT-treated mice. A third line of evidence for the involvement of ILCs comes from immunofluorescence analysis experiments detecting both CD90 and AREG which are found co-expressed by ILC2s. Pancreatic tissue sections illustrate the localization of high numbers of ILC2s in the chronically inflamed pancreas of DT-treated DEREG mice (**Fig. 5g**). We also evaluated the presence of both CD90 and amphiregulin in human chronic pancreatitis by studying in histology sections of pancreas tissue. The demonstration of double positive cells suggests involvement of ILC2 in pancreatic remodeling also in humans (**Fig. 5h**).

Tregs promote acinar cell regeneration and help to prevent loss of exocrine function

We next analyzed whether Treg-dependent expression of growth factors also affects acinar cell regeneration and the exocrine function of the pancreas in CP. Labeling of Ki67 and α-amylase in pancreatic sections of DT-treated mice showed a significant reduction in the number of proliferating acinar cells, compared to PBS-treated controls. This results in a loss of exocrine tissue (**Fig. 6b**). RT-qPCR analysis detected significantly reduced mRNA levels for genes encoding secretory proteins like α-amylase and T7-trypsinogen (Mus musculus RIKEN cDNA 2210010C04 gene) in pancreatic tissue (**Fig. 6c**). Finally, we observed that fecal elastase activity was decreased in DT-treated mice compared to PBS controls (**Fig. 6d**). The amount of fecal elastase is used in clinical practice as a diagnostic marker of pancreatic insufficiency[30]. Two weeks after caerulein treatment the body weight curves indicated a steady decline in the DT-treated animals but not in the PBS-treated control mice. This means that Tregs are required for the preservation and/or regeneration of pancreatic exocrine tissue and that Treg-mediated inhibition of the type 2 inflammation prevents significant weight loss in our CP model (**Fig. 6e**).

Discussion

In CP an inflammation-triggered process results in the progressive and irreversible destruction of functional pancreatic tissue and its replacement by fibrotic scar tissue[31]. Till today, a causal therapy or a strategy to limit disease progression are not available. For the progression of fibrosis, the interaction of pancreatic macrophages and stellate cells plays a crucial role[13,14,32]. The cytokines IL-4 and IL-13, mainly released by Th2 cells[33] and ILC2s [34], polarize macrophages towards alternatively activated macrophages[13]. In the present study we demonstrate that during CP, Tregs balance the immune response and limit the development of fibrosis by suppressing the type 2 immune response driven by alternative activated macrophages, Th2-cells and ILC2s. Alternatively activated macrophage differentiation seems to occurs in pancreatic tissue while Tregs and Th2-cells seems to be activated in lymphatic tissue during the course of chronic pancreatitis. A direct or indirect influence of Tregs on tissue repair, regeneration and fibrosis has been reported for various organs such as skin[35], muscle[36] and lung[37]. Tregs influence monocyte and neutrophil recruitment, macrophage polarization and T-effector cell differentiation[38] to regulate wound healing and tissue remodeling. In fibrotic lung as well as in liver diseases, Foxp3+/CD25+ Tregs limit fibrogenesis[37,39].

In our mouse model we demonstrate that during pancreatitis Tregs suppress the systemic type 2 immune response involving cells of the innate as well as the adaptive immune system. The depletion of Tregs results in a dramatically increased systemic Th2-response accompanied by increased cytokine levels of IL-13 and IL-10. In the spleen ILCs differentiate into ILC2 and we demonstrate an accumulation of ILC2 in the pancreas. In the damaged pancreas we observe a significant shift of macrophage polarization towards alternatively activated macrophages which might trigger excessive fibrosis and limit acinar cell regeneration. Alternatively activated macrophages, mainly described as M2-like macrophages, are known to regulate stellate cell activation and fibrosis[13] as well as organ regeneration and acinar cell differentiation[15,40]. In general, fibrogenesis and tissue regeneration processes are controlled by the release of growth factors and their counter regulators. Depletion of regulatory T-cells permits pancreatic CD206+ macrophages to release excessive amounts of various growth factors like TGFβ and FGF known to activate PSCs and to promote fibrosis[19]. Similarly activin, another growth factor of the TGF-superfamily, drives tissue fibrosis in chronic liver[41], kidney[42] and lung[43] diseases and has been reported to activate pancreatic stellate cells and fibroblasts[44]. Inhibin is closely related to activin but has opposite biological effects. Whereas activin, is a homodimer of inhibin βA subunits, inhibin is a heterodimer of inhibin βA with the more distantly-related α subunit. Macrophages, in response to damage associated molecular patterns (DAMP)-signals from damaged acinar cells, upregulate the transcript levels of inhibin βA while those of inhibin α were unchanged, promoting the formation of activin homo-dimers. Activin is known to induce PCSs to secrete extracellular matrix protein synergistically to the effects of TGFß[44]. It has also been shown that activin is released from PSCs after TGFß stimulation, which may start an autocrine activation loop. Another counter regulator of activin is follistatin, which blocks the interaction of activin with its receptor[45]. Follistatin, which is suppressed in the absence of Tregs, is known to inhibit the synthesis of collagen and TGFß in PSCs and thus terminates the activin autocrine loop[44]. Not only PSCs, but also acinar cells are sensitive to activin stimulation. The presence of activin during acinar cell differentiation suppresses the synthesis of secretory proteins and stops cell proliferation [46]. We assume that in DT-treated animals the observed expression changes of activin and follistatin affect the regeneration of acinar cells, which may explain the enhanced acinar to ductal metaplasia that we see in mice lacking Tregs. The imbalance between activin on the one hand and inhibin as well as follistatin on the other could contribute to tissue fibrosis and may limit acinar cell regeneration and differentiation.

As we have shown, Tregs are able to suppress the macrophage response and growth factor release and prevent uncontrolled tissue fibrosis in CP. Tregs control pancreatic macrophages, however another cell population of the innate immune system, namely the ILCs, could play a decisive role here. In our model, depletion of Tregs resulted in a significant accumulation of lin-/CD45+/CD127+/CD90+ cells in the pancreas. The expression of the transcription factor Gata3 characterizes these cells as ILC2s[47]. Tregs are able to suppress the proliferation of tissue resident ILCs in an IL2-dependent manner[48]. ILC2s in turn can stimulate the M2-like macrophage response via the release of IL-13[49,50]. ILC2s also express the growth factor amphiregulin[51], which was shown to be involved in the TGFβ mediated activation of lung fibrosis and regeneration processes. Amphiregulin is known to activate the epidermal growth factor receptor

(EGFR) family signaling pathway[52,53]. Many studies have identified the EGFR-pathway as a key pathway controlling the wound healing response[54–57]. Interestingly increased levels of amphiregulin are also found during coronavirus (SARS-CoV) infection, where many survivors develop pulmonary fibrosis. Comparable to our mouse model of CP, a dysregulated EGFR pathway has also been reported to associate with the development of pulmonary fibrosis-like disease after SARS-CoV infection[58].

In sum our data suggest that one important role of Tregs is to prevent uncontrolled fibrogenesis by repressing Th2-cells and ILC2-dependent M2-like macrophage polarization via IL-4/IL-13 release. Depletion of Tregs initiates a type 2 immune response accompanied by pronounced stellate cell activation and extracellular matrix protein production. It is interesting to note that despite the increased release of growth factors, damaged acinar cells do not regenerated. Apparently the strong fibrogenic stimulus suppresses the regeneration of the exocrine pancreatic tissue. For patients suffering from CP a tissue-preserving therapy would be fundamental in order to prevent exocrine and endocrine insufficiency. Our results implicate that Tregs can limit pancreatic fibrosis while stimulating acinar cell regeneration. Based on our results Tregs might represent a promising target for the development of a concept for the treatment of CP.

Methods

Animal model

DEREG mice (C57Bl/6 background, bacterial artificial chromosome-transgenic mice expressing a diphtheria toxin (DT) receptor-enhanced green fluorescent protein fusion protein under the control of the foxp3 gene locus, allowing selective and efficient depletion of Foxp3+ Treg cells by DT injection) were kindly provided by Jochen Huehn and have been previously described in detail in[27]. Wildtype C57Bl/6 mice were purchased from Charles River Laboratories (Sulzfeld, Germany). CP was induced by hourly repetitive caerulein i.p. injection (50µg/kg/bodyweight) (4030451, Bachem) over 6 hours, three times per week over a time period of four weeks. Tregs were depleted three times per week over the period of four weeks of caerulein treatment by 1 µg diphtheria toxin (DT) (D0564, Sigma Aldrich) i.p. injection one hour before the first caerulein dose. Control animals received phosphate buffered saline (PBS) instead of DT. This murine model is well established and results in a successful depletion of Tregs[25].

The body weight of the mice was determined over the whole four weeks. After that time all animals were sacrificed. Serum and organs were removed immediately and stored under different conditions for further experiments.

Antibodies

The following antibodies were used for immunofluorescence labeling and Flow-cytometry analysis: anti-GFP (ab6673, abcam), anti-CD3 (100202, BioLegend) anti-Mrc1/CD206 (OASA05048, aviva-sysbio), anti-αSMA (M0851, Dako), anti-CD90 (14-0900-85, Invitrogen), anti-Amphiregulin (sc-5796, SanatCruz), anti-

Amphiregulin (PA5-27298, Invitrogen), anti-collagen I (ab34710, abcam), anti-amylase (sc-46657, Santa Cruz), anti-Ki-67 (IHC-00375, Bethyl), anti-FGF Receptor (9740S, cell signaling), anti-InhibinβA (C9B1223, BioGenesis), anti-CD25-PE/Cy7 (102016, BioLegend), anti-CD4-PerCP/Cy5.5 (100433, BioLegend), anti-Cytokeratin 19 (ab15463, abcam), anti-CD4-PE (100408, BioLegend), anti-Tbet-Brilliant Violet 421 (644815, BioLegend), anti-Tbet-PerCP/Cy5.5 (644806, BioLegend), anti-GATA3-PE (653803, BioLegend), anti-Gata3-Brilliant Violet421 (653814, BioLegend), anti CD69-Brilliant Violet510 (104532, BioLegend), anti-CD11b-PerCP/Cy5.5 (101228, BioLegend), anti-CD206-APC (141708, BioLegend), anti-CD163-PE (12-1631-82, Invitrogen), anti-Ly6g-BV421 (127628, BioLegend), anti-lin-AlexaFlour700 (77923, BioLegend), anti-CD45-PerCP (103130, BioLegend), anti-CD90-Brilliant Violet605 (105343, BioLegend), anti-CD127-Brilliant Violet650 (135043, BioLegend), anti-GFAP-Alexa Fluor647 (51-9792-82, Invitrogen), anti-CD271-PE (12-9400-42, Invitrogen), anti-goat-Cy3 (705-165-147, Jackson ImmunoResearch), anti-mouse-FITC (115-095-146, Jackson ImmunoResearch), anti-mouse-Cy3 (115-165-166, Jackson ImmunoResearch), anti-mouse-Cy5 (115-175-146, Jackson ImmunoResearch), anti-rabbit-FITC (711-095-152, Jackson ImmunoResearch), anti-rabbit-Cy3 (111-165-144, Jackson ImmunoResearch), anti-rat-Cy3 (112-165-062, Jackson ImmunoResearch).

Flow cytometry analysis

Spleen was homogenized with a 70 µmcell strainer. Splenocytes were washed with PBS and centrifuged at 300g for 6min. The cell pellet was resuspended in 1mL 1x lysis buffer (10x buffer: 1.5M NH_4Cl, 0.1M $KHCO_3$, 10mM EDTA•2Na) and incubated for 5minutes at room temperature. The reaction was terminated with PBS.

Pancreatic tissue was dissociated with the Multi Tissue Dissociation Kit 1 (130-110-201, MiltenyiBiotec). First, the pancreas was transferred to serum-free DMEM and the enzyme mix. The tissue was homogenized with the gentleMACS Dissociator (130-093-235, MiltenyiBiotec) at 120runs for 37s. After incubation at 37°C for 20min under continuous rotation the samples were again dissociated at 168runs for 37s. Acinar cells and extracellular remains were removed by filtration through a 70µm cell strainer. Subsequently the suspension was centrifuged at 300g for 6min.

After washing with FACS buffer, $1x10^6$ cells per tube were pre-incubated with 1µL FcR Blocking Reagent (130-092-575, MiltenyiBiotec) to block non-specific Fc-mediated interactions. Next, extracellular markers (1:50 CD4, CD69 and CD25; 1:20 lin-, 1:50 CD90, CD127 and CD45; 1.50 CD11b, Ly6g, CD163, CD206, GFAP, CD271) were labeled by adding the antibody cocktail and incubated at 4°C for 30minutes. After fixation and permeabilization (Transcription Factor Staining Buffer Set, 130-122-981, Miltenyi Biotec) the cell suspensions were again treated with FcR Blocking Reagent and labeled with the intracellular antibody cocktail (1:10 Foxp3, Gata-3 and Tbet). Finally, the samples were analyzed by flow cytometry (BD, *LSRII*) and calculated by *FlowJo* (**supplement fig. 2**).

Histology, immunohistochemistry and immunofluorescence

Pancreas and lymph nodes were removed immediately from the sacrificed mice and fixed in 4.5% formaldehyde for paraffin embedding and for cryo-embedding in TissueTec.

Paraffin embedded tissue samples were cut in 2µm slides and afterwards used for Masson Goldner (100485, Merck Millipore) and Azan staining (12079, Morphisto).

Immunofluorescence labeling was performed from 2µm cryo slides. The antibodies were used in a 1:200 dilution and incubated over night at 4°C. The appropriate secondary antibody was used also in a 1:200 dilution, 1 hour at room temperature.

Human chronic pancreatitis tissue samples was collected in the context of the ChroPac trial (ISRCTN38973832)[59], staining of Areg and CD90 was performed like previously described for mouse tissue samples.

Serum Cytokine measurements

The serum cytokine concentration of IL6, IL4 and IL10 were measured by Cytometric Bead Array (CBA) Mouse inflammation kit (BD 552364, BD Bioscience, San Jose, CA, USA).

Fecal Elastase activity analysis in stool samples

Feces were resuspend in 500mmol/L NaCl, 100mmol/L $CaCl_2$ containing 0.1% Triton X-100 and two times sonicated. Fecal elastase activity was determined by fluorometric enzyme kinetic over 1 hour at 37°C by the usage of 0.12mM elastase substrate Suc-AAA-AMC (4006305.0050, Bachem) like previously described[12]. Kinetics were measured in 100mmol/l Tris buffer containing 5mmol/L $CaCl_2$ at pH 8.0.

Isolation of primary cells (BMDMs and acini)

Acini were isolated from mouse (C57Bl/6) pancreas by collagenase digestion under sterile conditions, as previously reported[6]. Cells were maintained and stimulated in Dulbecco's modified Eagle medium containing 10mM 4-(2-hydroxyethyl)-1-piperazine ethansulfonic acid (HEPES), 2% of bovine serum albumin (BSA) and 1% Penstrep. Stimulation of acinar cells was performed with 1µM CCK for 30min., afterwards cells were centrifuged for 30sec. at 500rpm and resuspended in fresh media to wash out residual CCK. BMDMs were isolated from femur and tibia of C57Bl/6 mice under sterile conditions as previously described[10,22]. Bone marrow was flushed out of the bones with sterile PBS and passed through a cell strainer (70µm). Cells were washed with sterile PBS, counted and maintained in 6-well plates in a concentration of 2.5 million cells/well with RPMI medium (1% Penstrep and 10% FCS). 6h after isolation from the bone marrow medium and non-attached cells were removed and cells were resuspended in fresh medium containing 20µg/ml M-CSF. After 5-7 days the cells were used for experiments. BMDMs and acini were co-incubated for 6h, afterward BMDMs were washed carefully to remove residual acini and total RNA was extracted from cells using TRIzol reagent, followed by column purification and quality control.

RNA Isolation and RT-qPCR analysis

The pancreas was removed and directly snap frozen in liquid nitrogen. Total RNA was extracted from pancreas tissue using TRIzol® Reagent (15596026, life technologies). Samples were treated with 500µL TRIzol® and homogenized with a TissueLyser. After addition of 100 µL Chloroform, samples were vortexed and centrifuged at 14000rpm, 15min at 4°C. Subsequently, the upper of the three resulting phases was transferred to a new tube. RNA was precipitated by adding 250µL isopropyl alcohol. The sample was incubated for 10 min at RT and centrifuged at 14000rpm, 10min, 4°C. The pellet was washed with 500µL 75% ethanol and centrifuged at 7500rpm for 10min at 4°C. After air-drying the pellet was solved in 100 µL A. dest.

RNA samples (2µg) were transcribed into complementary DNA (cDNA). The cDNA was synthesized using a standard protocol: 2µg RNA; 5µM OligodT primers; 75ng random primers; 0,5µM dNTP Mix; 1x First Strand Buffer (18080044, Invitrogen); 10µM DTT; 40 Units RNasin® Ribonuclease Inhibitor (N251B, Promega) and 200 Units M-MLV RT (28025013, invitrogen). The total volume per reaction was 20µL.

The expression of genes of interest was analyzed by reverse transcription-quantitative PCR (RT-qPCR) using the SYBR-green method. The qPCR amplification was performed in a volume of 5µL containing 1x SYBR® Green PCR Master Mix (4309155, applied biosystems), 300ng gene-specific oligonucleotide primers (reverse and forward) and a 1:10 dilution of cDNA fragments in two technical replicates. Detects transcript levels were normalized to *Rn5s* and to the relative expression in control mice. Quantitative mRNA alterations were determined using the $2^{-\Delta\Delta Ct}$-method.

RT-qPCR target gene	Forward primer sequence (5'-3')	Reverse primer sequence (5'-3')
Rn5s	GCCCGATCTCGTCTGATCTC	GCCTACAGCACCCGGTAT TC
Amy2a4	CAAAATGGTTCTCCCAAGGA	ACATCTTCTCGCCATTCCAC
Areg	CTGATCTTTGTCTCTGCCATCA	AGCCTCCTTCTTTCTTCTGTT
Col1a	CAGACTGGCAACCTCAAGAA	CAAGGGTGCTGTAGGTGAAG
Fgf1	GATGGCACCGTGGATGGGAC	AAGCCCTTCGGTGTCCATGG
Fst	AAAACCTACCGCAACGAATG	TTCAGAAGAGGAGGGCTCTG
Il10	TTGAATTCCCTGGGTGAGAAG	TCCACTGCCTTGCTCTTATTT
Il1b	GAGGACATGAGCACCTTCTTT	GCCTGTAGTGCAGTTGTCTAA
Inha	ATGCACAGGACCTCTGAACC	GGATGGCCGGAATACATAAG
Inhba	GATCATCACCTTTGCCGAGT	TGGTCCTGGTTCTGTTAGCC
Mrc1	GGCGAGCATCAAGAGTAAAGA	CATAGGTCAGTCCCAACCAAA
Tgfb1	CGAAGCGGACTACTATGCTAAA	TCCCGAATGTCTGACGTATTG
Trp7	CAACTACCCTTCACTCCTTCAG	TGCCTGGGTAAGAACTTGTG
Chil3	TCCAGAAGCAATCCTGAAGAC	GTCCTTAGCCCAACTGGTATAG
Acta2	GCCAGTCGCTGTCAGGAACCC	CCAGCGAAGCCGGCCTTACA

Transcriptome analysis of BMDMs

Microarray-based transcriptome analysis was performed as previously described[10,22]. Individual RNA samples were analysed using Affymetrix GeneChip Mouse Gene 2.0 ST Arrays and GeneChip WT PLUS

Reagent Kit (Thermo Fisher Scientific Inc., Waltham, MA) according to the manufacturer's instructions. Microarray data analysis was performed using the Rosetta Resolver software system (Rosetta Bio Software, Seattle, WA). Significantly different mRNA levels were defined using the following criteria: one-way ANOVA with Benjamini and Hochberg FDR ($p \leq 0.05$), signal correction statistics (Ratio Builder software) ($p \leq 0.05$), and an expression value ratio between the different conditions of 1.5-fold.

Declarations

Acknowledgments: The authors would like to thank Jochen Huehn for providing the DEREG mice. We also thank Kathrin Gladrow, Diana Krüger, Susi Wiche and Jenny Radel for their technical support.

Specific author contributions: Concept of the study MS, FUW, JG. Data acquisition and interpretation: JG, AW, AAA, MS, JG, GH, UV, BMB. Writing committee MS, FUW, JG, JM, MML. Correction of manuscript and approval of final version: all.

Funding: This work was supported by Deutsche Forschungsgemeinschaft (DFG SE 2702/2-1, SE 2702/2-3, AG 203/4-1, GRK 1947, DFG MA 4115/1-2/3, SFB1321: Project-ID 329628492), the PePPP center of excellence MV (ESF/14-BM-A55-0045/16) and the EnErGie/P2 Project (ESF/14-BM-A55-0008/18).

References

1. Ammann, R. W., Akovbiantz, A., Largiader, F. & Schueler, G. Course and outcome of chronic pancreatitis. Longitudinal study of a mixed medical-surgical series of 245 patients. *Gastroenterology* **86**, 820–828 (1984).

2. Ceyhan, G. O. *et al.* Pancreatic Neuropathy and Neuropathic Pain—A Comprehensive Pathomorphological Study of 546 Cases. *Gastroenterology* **136**, 177-186.e1 (2009).

3. Yadav, D. & Lowenfels, A. B. The epidemiology of pancreatitis and pancreatic cancer. *Gastroenterology* **144**, 1252–1261 (2013).

4. Singh, V. K., Yadav, D. & Garg, P. K. Diagnosis and Management of Chronic Pancreatitis: A Review. *JAMA* **322**, 2422–2434 (2019).

5. Mayerle, J. *et al.* Genetics, Cell Biology, and Pathophysiology of Pancreatitis. *Gastroenterology* **156**, 1951-1968.e1 (2019).

6. Sendler, M. *et al.* Cathepsin B Activity Initiates Apoptosis via Digestive Protease Activation in Pancreatic Acinar Cells and Experimental Pancreatitis. *J. Biol. Chem.* **291**, 14717–14731 (2016).

7. Halangk, W. *et al.* Role of cathepsin B in intracellular trypsinogen activation and the onset of acute pancreatitis. *J. Clin. Invest.* **106**, 773–781 (2000).

8. Gukovsky, I., Gukovskaya, A. S., Blinman, T. A., Zaninovic, V. & Pandol, S. J. Early NF-kappaB activation is associated with hormone-induced pancreatitis. *Am. J. Physiol.* **275**, G1402-1414 (1998).

9. Sendler, M. *et al.* Tumour necrosis factor α secretion induces protease activation and acinar cell necrosis in acute experimental pancreatitis in mice. *Gut* **62**, 430–439 (2013).

10. Sendler, M. *et al.* Cathepsin B-Mediated Activation of Trypsinogen in Endocytosing Macrophages Increases Severity of Pancreatitis in Mice. *Gastroenterology* **154**, 704-718.e10 (2018).

11. Gukovskaya, A. S. *et al.* Neutrophils and NADPH oxidase mediate intrapancreatic trypsin activation in murine experimental acute pancreatitis. *Gastroenterology* **122**, 974–984 (2002).

12. Sendler, M. *et al.* Complement Component 5 Mediates Development of Fibrosis, via Activation of Stellate Cells, in 2 Mouse Models of Chronic Pancreatitis. *Gastroenterology* **149**, 765-776.e10 (2015).

13. Xue, J. *et al.* Alternatively activated macrophages promote pancreatic fibrosis in chronic pancreatitis. *Nat Commun* **6**, 7158 (2015).

14. Wu, J. *et al.* Macrophage phenotypic switch orchestrates the inflammation and repair/regeneration following acute pancreatitis injury. *EBioMedicine* **58**, 102920 (2020).

15. Criscimanna, A., Coudriet, G. M., Gittes, G. K., Piganelli, J. D. & Esni, F. Activated macrophages create lineage-specific microenvironments for pancreatic acinar- and β-cell regeneration in mice. *Gastroenterology* **147**, 1106-1118.e11 (2014).

16. Rappolee, D. A., Mark, D., Banda, M. J. & Werb, Z. Wound macrophages express TGF-alpha and other growth factors in vivo: analysis by mRNA phenotyping. *Science* **241**, 708–712 (1988).

17. Nascimento, D. C. *et al.* IL-33 contributes to sepsis-induced long-term immunosuppression by expanding the regulatory T cell population. *Nat Commun* **8**, 14919 (2017).

18. Wynn, T. A. & Vannella, K. M. Macrophages in Tissue Repair, Regeneration, and Fibrosis. *Immunity* **44**, 450–462 (2016).

19. Apte, M. V. *et al.* Pancreatic stellate cells are activated by proinflammatory cytokines: implications for pancreatic fibrogenesis. *Gut* **44**, 534–541 (1999).

20. Bachem, M. G. *et al.* Identification, culture, and characterization of pancreatic stellate cells in rats and humans. *Gastroenterology* **115**, 421–432 (1998).

21. Gieseck, R. L., Wilson, M. S. & Wynn, T. A. Type 2 immunity in tissue repair and fibrosis. *Nat. Rev. Immunol.* **18**, 62–76 (2018).

22. Sendler, M. *et al.* NLRP3 Inflammasome Regulates Development of Systemic Inflammatory Response and Compensatory Anti-Inflammatory Response Syndromes in Mice With Acute Pancreatitis.

Gastroenterology **158**, 253-269.e14 (2020).

23. Sakaguchi, S., Sakaguchi, N., Asano, M., Itoh, M. & Toda, M. Immunologic self-tolerance maintained by activated T cells expressing IL-2 receptor alpha-chains (CD25). Breakdown of a single mechanism of self-tolerance causes various autoimmune diseases. *J Immunol* **155**, 1151–1164 (1995).

24. Sakaguchi, S., Wing, K., Onishi, Y., Prieto-Martin, P. & Yamaguchi, T. Regulatory T cells: how do they suppress immune responses? *Int Immunol* **21**, 1105–1111 (2009).

25. Tiemessen, M. M. *et al.* CD4+CD25+Foxp3+ regulatory T cells induce alternative activation of human monocytes/macrophages. *Proceedings of the National Academy of Sciences* **104**, 19446–19451 (2007).

26. Watanabe, T., Kudo, M. & Strober, W. Immunopathogenesis of pancreatitis. *Mucosal Immunol* **10**, 283–298 (2017).

27. Lahl, K. *et al.* Selective depletion of Foxp3+ regulatory T cells induces a scurfy-like disease. *J. Exp. Med.* **204**, 57–63 (2007).

28. Mchedlidze, T. *et al.* Interleukin-33-Dependent Innate Lymphoid Cells Mediate Hepatic Fibrosis. *Immunity* **39**, 357–371 (2013).

29. Hams, E. *et al.* IL-25 and type 2 innate lymphoid cells induce pulmonary fibrosis. *Proceedings of the National Academy of Sciences* **111**, 367–372 (2014).

30. Frost, F. *et al.* Impaired Exocrine Pancreatic Function Associates With Changes in Intestinal Microbiota Composition and Diversity. *Gastroenterology* **156**, 1010–1015 (2019).

31. Beyer, G., Habtezion, A., Werner, J., Lerch, M. M. & Mayerle, J. Chronic pancreatitis. *Lancet* **396**, 499–512 (2020).

32. Haber, P. S. *et al.* Activation of pancreatic stellate cells in human and experimental pancreatic fibrosis. *Am. J. Pathol.* **155**, 1087–1095 (1999).

33. Ansel, K. M., Djuretic, I., Tanasa, B. & Rao, A. Regulation of Th2 differentiation and Il4 locus accessibility. *Annu Rev Immunol* **24**, 607–656 (2006).

34. Noval Rivas, M., Burton, O. T., Oettgen, H. C. & Chatila, T. IL-4 production by group 2 innate lymphoid cells promotes food allergy by blocking regulatory T-cell function. *J Allergy Clin Immunol* **138**, 801-811.e9 (2016).

35. Kalekar, L. A. *et al.* Regulatory T cells in skin are uniquely poised to suppress profibrotic immune responses. *Sci Immunol* **4**, (2019).

36. Burzyn, D. *et al.* A special population of regulatory T cells potentiates muscle repair. *Cell* **155**, 1282–1295 (2013).

37. Kotsianidis, I. *et al.* Global Impairment of CD4 $^{+}$ CD25 $^{+}$ FOXP3 $^{+}$ Regulatory T Cells in Idiopathic Pulmonary Fibrosis. *Am J Respir Crit Care Med* **179**, 1121–1130 (2009).

38. Li, J., Tan, J., Martino, M. M. & Lui, K. O. Regulatory T-Cells: Potential Regulator of Tissue Repair and Regeneration. *Front Immunol* **9**, 585 (2018).

39. Claassen, M. A. A., de Knegt, R. J., Tilanus, H. W., Janssen, H. L. A. & Boonstra, A. Abundant numbers of regulatory T cells localize to the liver of chronic hepatitis C infected patients and limit the extent of fibrosis. *J Hepatol* **52**, 315–321 (2010).

40. Criscimanna, A. *et al.* Duct cells contribute to regeneration of endocrine and acinar cells following pancreatic damage in adult mice. *Gastroenterology* **141**, 1451–1462, 1462.e1–6 (2011).

41. Patella, S., Phillips, D. J., Tchongue, J., de Kretser, D. M. & Sievert, W. Follistatin attenuates early liver fibrosis: effects on hepatic stellate cell activation and hepatocyte apoptosis. *Am J Physiol Gastrointest Liver Physiol* **290**, G137-144 (2006).

42. Yamashita, S., Maeshima, A., Kojima, I. & Nojima, Y. Activin A is a potent activator of renal interstitial fibroblasts. *J Am Soc Nephrol* **15**, 91–101 (2004).

43. Hardy, C. L. *et al.* The activin A antagonist follistatin inhibits cystic fibrosis-like lung inflammation and pathology. *Immunol Cell Biol* **93**, 567–574 (2015).

44. Ohnishi, N. *et al.* Activin A is an autocrine activator of rat pancreatic stellate cells: potential therapeutic role of follistatin for pancreatic fibrosis. *Gut* **52**, 1487–1493 (2003).

45. Walton, K. L., Johnson, K. E. & Harrison, C. A. Targeting TGF-β Mediated SMAD Signaling for the Prevention of Fibrosis. *Front Pharmacol* **8**, 461 (2017).

46. Yasuda, H. *et al.* Activin A: negative regulator of amylase secretion and cell proliferation in rat pancreatic acinar AR42J cells. *Am J Physiol* **267**, G220-226 (1994).

47. Hoyler, T. *et al.* The transcription factor GATA-3 controls cell fate and maintenance of type 2 innate lymphoid cells. *Immunity* **37**, 634–648 (2012).

48. Gasteiger, G., Fan, X., Dikiy, S., Lee, S. Y. & Rudensky, A. Y. Tissue residency of innate lymphoid cells in lymphoid and nonlymphoid organs. *Science* **350**, 981–985 (2015).

49. Lechner, A. J. *et al.* Recruited Monocytes and Type 2 Immunity Promote Lung Regeneration following Pneumonectomy. *Cell Stem Cell* **21**, 120-134.e7 (2017).

50. Bouchery, T. *et al.* ILC2s and T cells cooperate to ensure maintenance of M2 macrophages for lung immunity against hookworms. *Nat Commun* **6**, 6970 (2015).

51. Krishnamoorthy, N. *et al.* Cutting edge: maresin-1 engages regulatory T cells to limit type 2 innate lymphoid cell activation and promote resolution of lung inflammation. *J Immunol* **194**, 863–867 (2015).

52. Berasain, C. *et al.* Amphiregulin: an early trigger of liver regeneration in mice. *Gastroenterology* **128**, 424–432 (2005).

53. Zhou, Y. *et al.* Amphiregulin, an epidermal growth factor receptor ligand, plays an essential role in the pathogenesis of transforming growth factor-β-induced pulmonary fibrosis. *J Biol Chem* **287**, 41991–42000 (2012).

54. Tokumaru, S. *et al.* Ectodomain Shedding of Epidermal Growth Factor Receptor Ligands Is Required for Keratinocyte Migration in Cutaneous Wound Healing. *Journal of Cell Biology* **151**, 209–220 (2000).

55. Repertinger, S. K. *et al.* EGFR Enhances Early Healing After Cutaneous Incisional Wounding. *Journal of Investigative Dermatology* **123**, 982–989 (2004).

56. Chen, J. *et al.* EGFR Signaling Promotes TGF *β* -Dependent Renal Fibrosis. *JASN* **23**, 215–224 (2012).

57. Fuchs, B. C. *et al.* Epidermal growth factor receptor inhibition attenuates liver fibrosis and development of hepatocellular carcinoma: Fuchs et al. *Hepatology* **59**, 1577–1590 (2014).

58. Venkataraman, T., Coleman, C. M. & Frieman, M. B. Overactive Epidermal Growth Factor Receptor Signaling Leads to Increased Fibrosis after Severe Acute Respiratory Syndrome Coronavirus Infection. *J Virol* **91**, (2017).

59. Diener, M. K. *et al.* Partial pancreatoduodenectomy versus duodenum-preserving pancreatic head resection in chronic pancreatitis: the multicentre, randomised, controlled, double-blind ChroPac trial. *Lancet* **390**, 1027–1037 (2017).

Figures

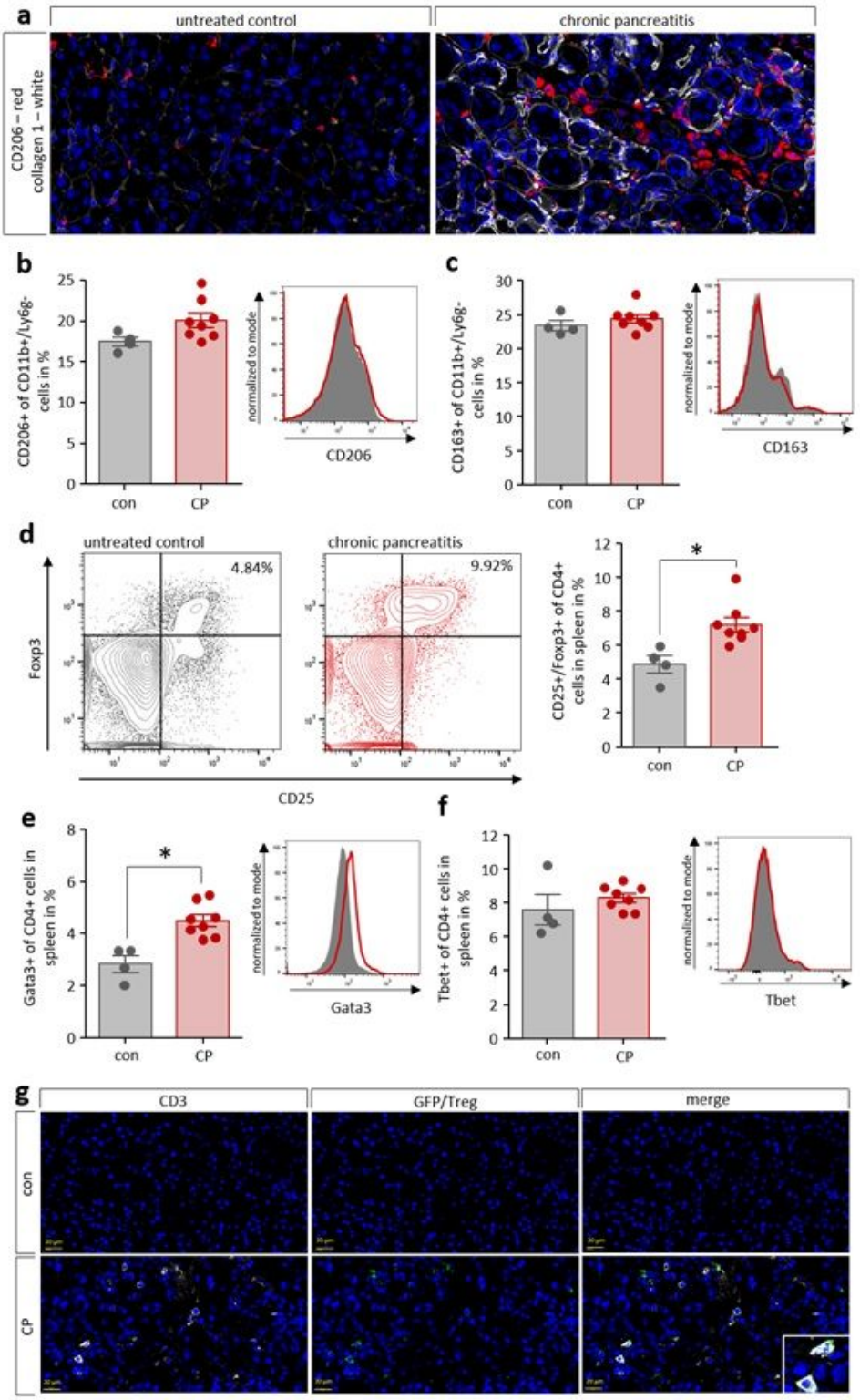

Figure 1

Chronic pancreatitis was induced in C57BL/6 mice by repetitive caerulein i.p. injection over 4 weeks. Labeling of CD206 and collagen 1 demonstrates fibrosis as well as increased numbers of alternatively activated macrophages in pancreatic tissue (a). No CP-dependent increase of splenic CD206- or CD163-positive macrophages is detectable by flow cytometry analysis showed (b, c). In contrast to the cells belonging to the innate immune system, the number of CD25+/Foxp3+/CD4+ Tregs is significantly

increased (d). The Th1/Th2 balance is also affected in CP, resulting in increased numbers of Gata3+ Th2 cells, whereas Tbet+ Th1 cells are not increased (e, f). Analysis of DTR-eGFP transgene expression in DT-untreated DEREG mice and untreated control animals (con) demonstrates sporadic CD3+/GFP+ cells exclusively in pancreatic sections of CP animals (g). All graphs represent n=4 or more animals per group. Statistically significant differences were tested by unpaired students t-test for independent samples and significance levels of $p<0.05$ are marked by an asterisk.

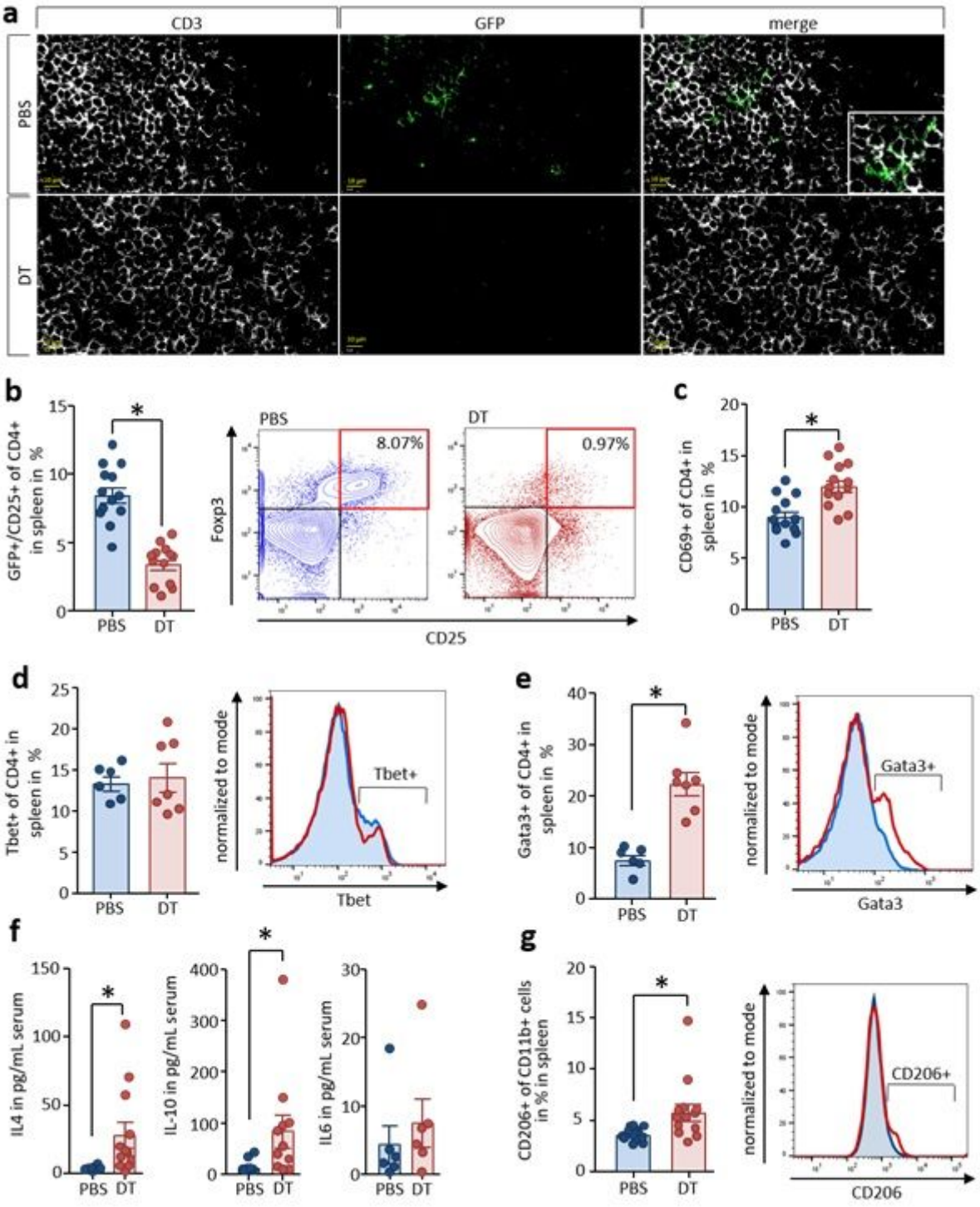

Figure 2

CP was induced in DEREG mice by repetitive caerulein i.p. injection over 4 weeks in Treg-depleted animals. Control mice received PBS instead of DT. An anti-GFP antibody was used for immunofluorescence staining of GFP+ Tregs in lymph node, scale bars represent 10 µm (a). Determination of GFP+ and CD25+ splenocytes was performed by flow cytometry (b). T-effector cell activation was measured by detection of CD69 on CD4+ T-cells (c). Furthermore, the T effector differentiation of CD4+ splenocytes were quantified by flow cytometry. The T effector immune response was measured by intracellular staining of Tbet and Gata3 in CD4+ cells (d, e). Detected levels of the transcription factor Tbet were not significantly different between both groups. In contrast to the Th1 immune response, the Th2 immune response, as hallmarked by the presence of Gata3, was increased by depletion of regulatory T cells during CP. Measurement of serum cytokines by a cytometric bead array showed an increase of type 2cytokines like IL10 and IL4, whereas typical type 1cytokines like IL6 were not affected (f). Analysis of the surface marker CD206 on CD11b+ cells in the spleen by flow cytometry indicates that not only the Th2 response was increased but also the number of alternatively activated anti-inflammatory macrophages. (g). All results shown are based on 6 or more animals per experimental group. Statistically significant differences were tested by unpaired students t-test for independent samples and significance levels of $p<0.05$ are marked by an asterisk.

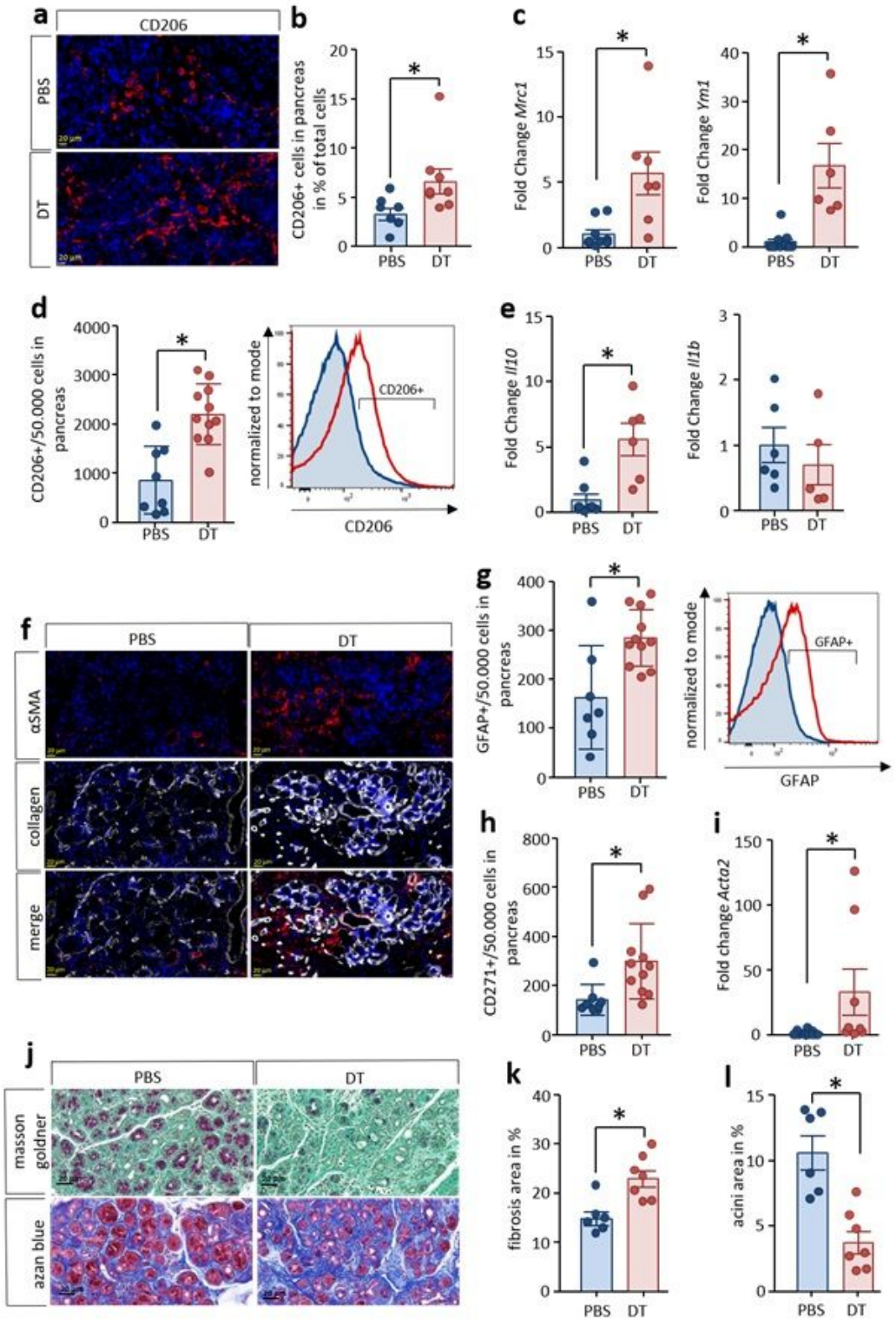

Figure 3

An increased type 2immune response is observed in the pancreas of DT-treated mice. Staining of pancreatic CD206+ macrophages reveals that their numbers were significantly elevated in DT treated animals (a, b). Gene expression analysis by RT-qPCR confirmed elevated expression of Mrc1 and Ym1 encoding anti-inflammatory macrophage markers (c). Flow cytometry analysis of leukocytes isolated from pancreatic tissue provides evidence for increased alternatively activated M2 macrophages in DT-

treated mice (d). Gene expression analysis by RT-qPCR demonstrates increased transcript levels for the anti-inflammatory cytokine IL10 whereas mRNA amounts of the pro-inflammatory IL1β cytokine are not affected (e). M2-like macrophages in DT-treated mice trigger pancreatic stellate cells (PSC), as shown by staining of αSMA and collagen 1 (f). Flow cytometry analysis of dissociated pancreatic tissue reveals a significant higher number of GFAP+ and CD271+ cells (g, h), and gene expression analysis of αSMA confirms activation of PSC after depletion of Tregs during CP (i). Finally, the higher PSC number causes increased fibrosis and pronounced loss of acinar cells (j), scale bars represent 100 µm. Quantitative analyses performed by Masson Goldner and Azan blue staining demonstrate a significant increase in fibrosis accompanied by decreased acinar cell numbers in the absence of Tregs (k, l). All results shown are based on 6 or more animals per group. Statistically significant differences were tested by unpaired students t-test for independent samples and significance levels of $p<0.05$ are marked by an asterisk.

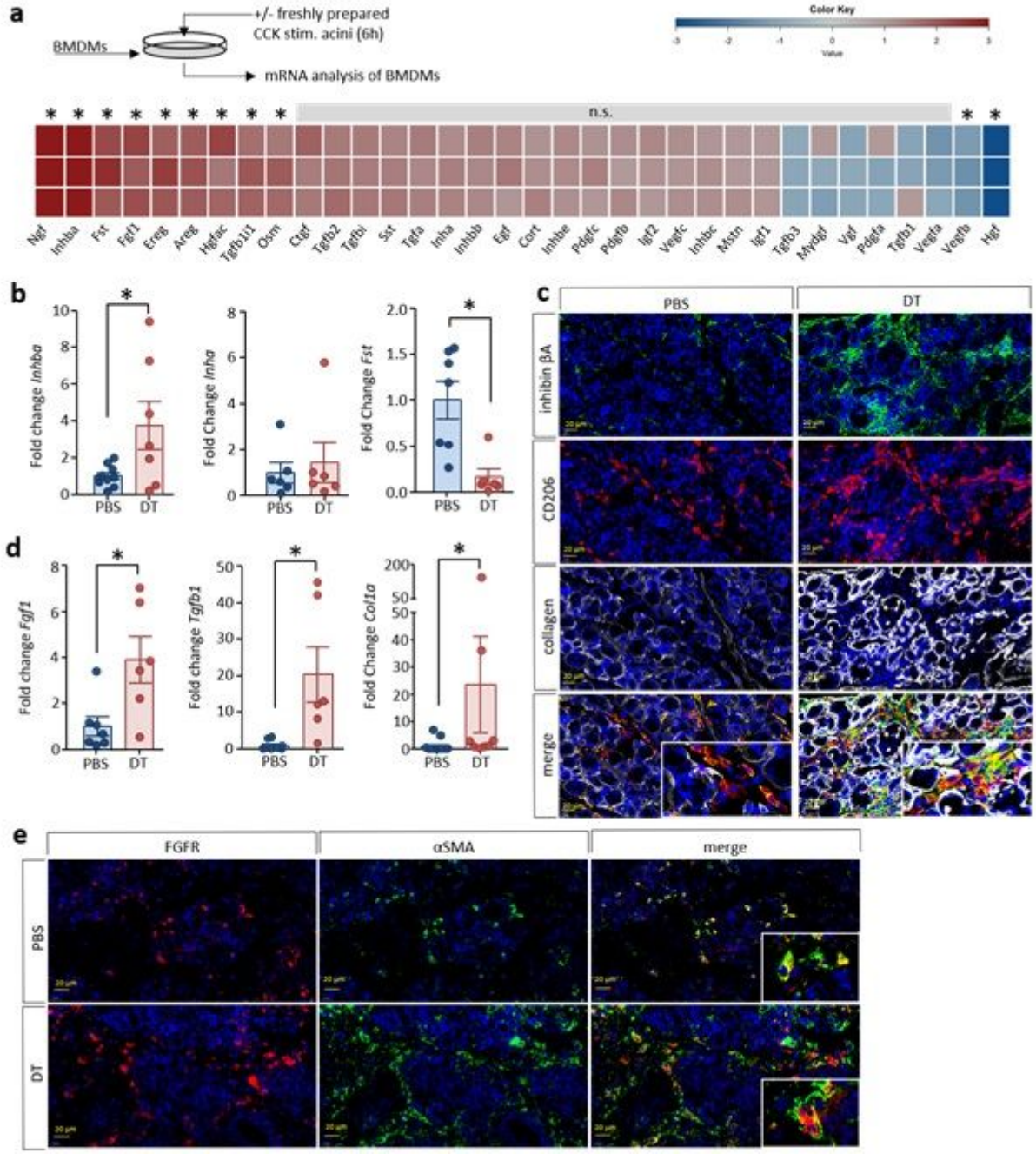

Figure 4

Pancreatic macrophages release a panel of growth factors regulating organ fibrosis. Bone marrow derived macrophages were isolated from C57Bl/6 mice and co-incubated with CCK-stimulated acini for 6h. Total RNA was isolated from BMDMs and transcriptome profiling was performed using Affymetrix GeneChip Mouse Gene 2.0 ST Arrays. Expression changes of genes encoding growth factors are visualized by a heat map (a). The gene-specific transcript levels of Ngf, Inhba, Fst, Fgf1, Ereg, and Areg encoding Nerve growth factor, inhibin A subunit β, follistatin, fibroblast growth factor 1, epiregulin, and amphiregulin, respectively, were significantly increased in BMDMs after co-incubation with acini (a). Growth factor gene expression was also investigated in pancreatic tissue from DEREG mice +/- DT by RT-qPCR. Expression of Inhba encoding Inhibin βA was significantly increased in DT-treated mice whereas transcript levels of Inha encoding inhibin α were not affected. Expression of Fst encoding follistatin was significantly decreased in DT-treated mice (b). Immunofluorescence labelling of inhibin βA and CD206 demonstrates co-localisation (c). Gene expression of growth factors FGF1 and TGFB was also upregulated in the pancreas of DT-treated mice and an higher expression of collagen 1 was shown by immunofluorescence labelling and RT-qPCR (c, d). Additional labelling of the FGF-receptor on α-SMA+ PSCs demonstrates increased fibrogenesis in DT-treated mice (e). Significantly differential mRNA levels as detected by microarray-based transcriptome analysis were defined using the following criteria: one-way ANOVA with Benjamini and Hochberg false discovery rate ($p \leq .05$), signal correction statistics (Ratio Builder software; $p \leq .05$), and an expression value ratio between the different conditions ≥1.5-fold (n=3). All results shown are based on 6 or more animals per group. Statistically significant differences were tested by unpaired students t-test for independent samples and significance levels of $p<0.05$ are marked by an asterisk.

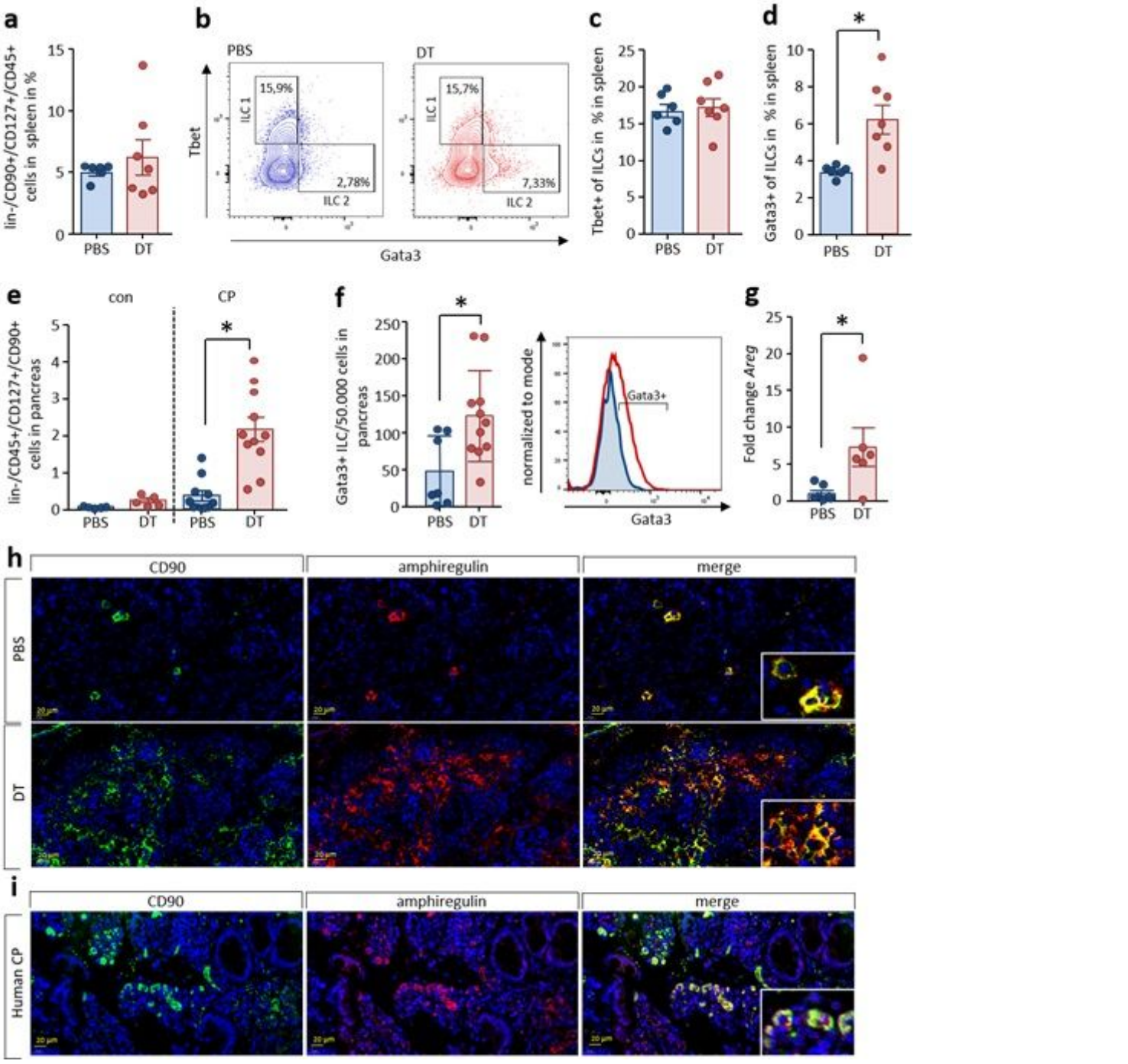

Figure 5

ILC2 are suppressed by regulatory T-cells. Splenocytes of CP animals, additionally treated with DT or PBS were isolated and analyzed by flow cytometry. The fraction of ILCs was discriminated as lin-/CD45+/CD127+/CD90+ cells (a). The presence of the transcription factors Gata3 and Tbet was used to differentiate ILC1 and ILC2 (b). Treg depletion increases the number of Gata3+ ILC2 but not of Tbet+ ILC1 in spleen (c, d). Isolated leukocytes from CP tissue of mice were investigated for pancreatic ILCs. The total number of lin-/CD45+/CD127+/CD90+ cells was dramatically increased in the absence of Tregs (e), and the number of Gata3+ ILC2 was significantly increased (f). Expression analysis of Areg encoding amphiregulin in pancreatic tissue by RT-qPCR confirms an increase in Treg-depleted animals during CP

(g). Transcript levels as determined by RT-qPCR were normalized using Rn5s as internal calibrator gene and were related to the corresponding mRNA amounts in control mice. Representative immunofluorescence labeling of CD90+ AREG+ detected AREG in pancreatic ILC2 from CP animals as well as in human tissue sections, scale bars represent 20µm (h, i). All results shown are based on 6 or more animals per group. Statistically significant differences were tested by unpaired students t-test for independent samples and significance levels of $p<0.05$ are marked by an asterisk.

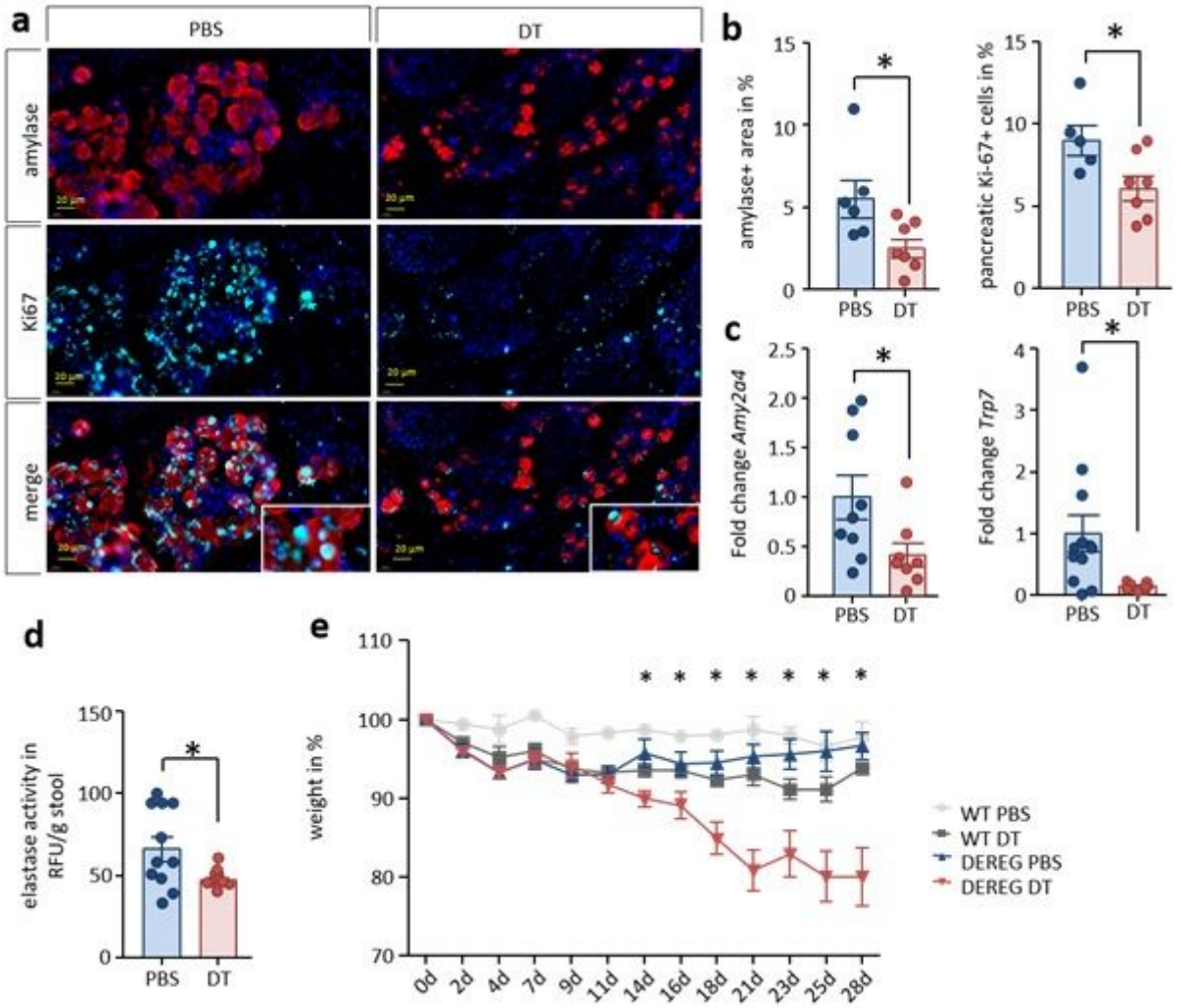

Figure 6

Treg-Depletion causes loss of exocrine function. Immunofluorescence labeling of α-amylase and Ki-67 indicates less proliferating acinar cells in the Treg depleted group. Scale bars represent 20µm (a). Quantification of the immunofluorescent labeling confirmed a significantly reduced number of acinar cells and less proliferating Ki67+ acinar cells in the pancreas of DT-treated mice (b). Gene expression of the pancreatic digestive enzymes amylase and trypsinogen as determined by RT-qPCR was significantly decreased during CP and depletion of Tregs (c). The activity of fecal elastase, a clinical marker of exocrine function, was also significantly decreased in DT-treated mice (d). The decreased exocrine pancreas function is furthermore reflected in body weight loss. Treg depletion in CP animals significantly increases the weight loss over time (e). All results shown are based on 6 or more animals per group.

Statistically significant differences were tested by unpaired students t-test for independent samples and one-way ANOVA, Bonferroni posttest, significance levels of $p<0.05$ are marked by an asterisk.

Supplementary Files

This is a list of supplementary files associated with this preprint. Click to download.

- FigureS1.jpg
- FigureS2.jpg